

FLUIDIC CAPACITANCE MODEL OF CAPILLARY-DRIVEN STOP VALVES

Jun Zeng

Microcosm Technologies Inc.
215 First Street, Cambridge MA 02142
e-mail: jzeng@memcad.com

Ken B. Greiner

Microcosm Technologies Inc.
215 First Street, Cambridge MA 02142
e-mail: ken@memcad.com

Manish Deshpande

Microcosm Technologies Inc.
215 First Street, Cambridge MA 02142
e-mail: manish@memcad.com

John R. Gilbert

Microcosm Technologies Inc.
215 First Street, Cambridge MA 02142
e-mail: jrg@memcad.com

ABSTRACT

This paper presents current research in design analysis of passive micro-fluidic stop valves driven by capillary forces. Capillary valves are used in controlling the liquid position by presenting a capillary pressure barrier due to a sudden change in cross-section. Valves of this type have multiple advantages on precise control in micro-fluidic devices over conventional ones.

In the design of a device employing such valves, a model describing the behavior of these valves is highly desirable. In this paper, we describe the extraction of this model using numerical techniques validated with experiment. The numerical analyses are conducted in FlumeCAD, a design and analysis tool for micro-fluidic devices. The detailed analyses yield a fluidic capacitance model for the capillary-driven valves. Devices that are pneumatically pressurized and driven by centrifugal force are studied in this paper. The methodology presented in this article can, in principle, be applied to a wide range of devices and actuation mechanisms.

INTRODUCTION

There is a wide interest in micron-scale integrated chemical/biochemical analysis or synthesis systems, also referred to as lab-on-a-chip. Sample injection and localization are two essential functions required in such devices as samples must be first injected into the system and properly routed to a specific reaction chamber (Harrison et al 1998, van den Berg et al 2000). These two functions can be accomplished for example using a series of valves that control the extent and flow of the sample. Other applications that micro-valves can be used to enhance on-chip chemical processing include improving the storage of reagents, priming of channels, switching of liquid flow-streams as well as isolating specific areas of the chip during sensitive steps in the chemical processing to prevent leakage and pressure fluctuations. From the device-design point

of view, such valves are required to be easily connected to the fluidic networks, and also be able to bear high liquid pressure.

Conventional diaphragm valves can fulfill this task, but require both moving parts and an external actuation mechanism, which often complicate the implementation and integration. Electro-kinetic methods to control the liquid have also been demonstrated (Bousse et al 1999). These methods are however sensitive to the physicochemical properties of the components and by the presence of trapped air.

An alternative approach presented in this paper uses a passive micro-fluidic capillary-driven valve that exploits the surface tension force to stop flows in micro-channels. The principle of operation is based on the pressure barrier that develops when the cross section of the capillary expands abruptly. These valves have the advantage of not requiring moving parts. They are not sensitive to the properties of the buffer/samples pumped or the presence of trapped air bubbles. They also alleviate problems associated with Joule heating that occur in electro-kinetic systems that demand high field strengths. Valves of this type recently have attracted considerable attention (Man et al 1998, Moroney et al 1999, Duffy et al 1999, Zeng et al 2000) and present strong appeal for applications to various micro-fluidic systems.

An in-depth understanding of the operating characteristics of such devices is necessary for component design and system integration. Numerical simulation provides quantitative analysis of different aspects of devices, and significant insight into the physics that is present in the components. The simulation process is gaining acceptance amongst MEMS researchers and engineers and is even regarded as means to interpret experimental data (Hsing et al 2000). Numerical simulation also provides a mechanism of exploring the entire parameter space

that influences the performance of a device, which is relatively hard experimentally. Simulation-based design analysis is broadly recognized as a cost-effective approach to device designs, it “can avoid costly, iterative experimental design process where components are fabricated, tested, and then redesigned to improve performance” (Jensen 2000).

Several researchers have employed computational fluid dynamics (CFD) in understanding the behavior of micro-fluidic components, both in pressure driven flow (Olsson et al 1999) as well as in electro-kinetics (Patankar et al 1998, Ermakov et al 1998). In these analyses the liquid buffer was assumed to fill the entire device therefore only single-phase fluid was concerned. The capillary-driven micro-fluidic valves employ a liquid/air interface as the active mechanism of affecting the fluid flow. Therefore modeling such device requires a multi-phase-fluids CFD solver. A Volume-of-Fluids (VOF) approach (Hirt et al 1981) is integrated into FlumeCAD to solve the multiphase flow problem. Detailed simulations using this approach are presented in this paper.

Capillary stop valves can be employed effectively in several systems. These include pressure driven systems (Moroney et al 1998) as well as rotating CDs where centrifugal force provides the necessary pressure (Duffy et al 1999). As the meniscus (interface) area/volume enlarges with increasing driving pressure, the increase in interfacial surface energy appears as an equivalent capacitance in the fluidic circuit. This fluidic capacitance relates meniscus volume to driving pressure in the similar fashion as electrical capacitance relates charge to voltage.

The objective of this article is to present the development of a meniscus capacitance model to represent the behavior of the stop valve. Such a capacitance model requires the relation between the charge (driving pressure) and response (volume of the meniscus). When the driving pressure exceeds a specific breaking point - the maximum capillary barrier - a fluid flow will be established through this micro-fluidic valve shorting the fluidic capacitance. The maximum capillary barrier defines the

ceiling criterion of the capacitance working relation, another essential component of the fluidic capacitance model.

The methodology of developing such a capacitance model is illustrated through two examples. Modeling of devices driven by liquid pressure is used to show means to establish the working relation between driving pressure and volume of meniscus. Simulations of centrifugal-driven devices are used to demonstrate means to derive the working limitation of the capacitance model. The geometrical factors are of primary concerns in both examples. It should be noted that the methodology presented in this article can be applied to every mechanical aspect of micro-fluidic valves and to valves with various driving mechanisms.

THEORY

A schematic of the capillary-driven gating operation is shown in Fig. 1. A narrow channel connects two large containers: a reservoir full of sample liquid and a reaction chamber initially empty. The pressure in the reservoir is higher, driving the sample from the reservoir to the reaction chamber. The liquid is prevented from entering the reaction chamber by the capillary force at the opening to the reaction chamber. This is called the “capillary barrier”. When the liquid pressure at the meniscus overcomes this maximum capillary barrier, the liquid will burst into the chamber and “short” the capillary valve. Precise control of the liquid sample position is thus enabled by tuning the driving force, be it pressure gradient, pneumatics, electro-kinetics or centrifugal force.

The channel is assumed to be a pipe with a circular opening of diameter D for simplicity. Consequently the height of the meniscus H is chosen to represent the meniscus volume. Assuming the ambient air pressure zero, the pressure drop across the meniscus may be expressed as

$$P_m = \gamma_{la} \epsilon$$

where γ_{la} is the surface tension coefficient (surface energy per unit area between liquid and air) and ϵ the local curvature of the interface. At steady state the interface should be part of the spherical surface required to maintain constant curvature therefore constant pressure distribution to avoid flow. This yields the expression of the local curvature as

$$\epsilon = \frac{16H}{D^2 + 4H^2}.$$

Therefore the working relation between the charge and the response can be expressed as

$$H = \frac{2\gamma_{la}}{P_m} \left(1 - \sqrt{1 - \left(\frac{DP}{4\gamma_{la}} \right)^2} \right). \quad (1)$$

Thermodynamics in terms of interfacial free energy is applied to estimate the maximum capillary barrier (Man et al 1998, Kim et al 1997). The total interfacial energy at the liquid front U_T may be expressed as

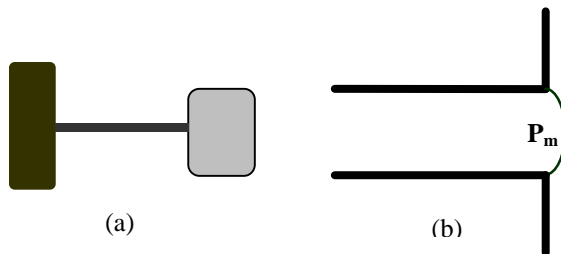


Figure 1. Schematic of capillary-driven gating operation. (a) shows top view of a μ Tas device. The reservoir and channel are filled by liquid sample (black). Pressure in the reservoir is higher and attempts to drive liquid into reaction chamber (gray). (b) shows a close-up view of the abruptly-expanding opening. Liquid pressure at the meniscus is P_m .

$$U_T = A_{sl}g_{sl} + A_{sa}g_{sa} + A_{la}g_{la}$$

where A_{sl} , A_{sa} and A_{la} are solid-liquid, solid-air, and liquid-air interface areas, and γ_{sl} , γ_{sa} and γ_{la} its corresponding surface energies per unit area which are related by Young's equation

$$g_{sa} = g_{sl} + g_{la} \cos \theta_c$$

where θ_c is the equilibrium (static) contact angle. Based on above, the maximum capillary barrier can be expressed as

$$P_{cb} = \frac{dU_T}{dV_l} = \frac{4g_{la} \sin \theta_c}{D} \quad (2)$$

where V_l is the liquid sample volume. Equation (2) gives the ceiling criterion. When the applied charge exceeds P_{cb} , a liquid flow will be established and the fluidic capacitance will be "shorted".

It should be noted that the theoretical analysis neglects the liquid momentum. In reality, however, the meniscus oscillates with noticeable kinetic energy. Consequently the viscous dissipation should also be taken into account. Therefore it is not entirely true to assume that the input energy $P_{cb}V_l$ transform to surface energy U_T completely. Further the existence of meniscus oscillation also has impact on local contact angle θ_c , which influences the shape of the meniscus. Last but not least, the theoretical analysis is limited to pipe flow. For channels with

different geometrical cross-section, a hydraulic diameter may not be adequate to compensate for the geometrical factor, which may introduce bias to its estimation.

Due to reasons stated above, theoretical analysis may not be adequate for design purpose in which much higher accuracy is desired. On the other hand, numerical simulation intends to replicate the real physics and account for all factors possible therefore is capable of supplying quantitative analyses with higher accuracy.

COMPUTATIONAL MODELING

The numerical method uses a VOF technique (Hirt et al 1981) to simulate the interface motion. The VOF method introduces an additional variable, the *volume-of-fluid* (F), that covers the entire computational region of interest. For each control volume, F denotes the fraction of that volume that is occupied by liquid and varies with time and position to accurately trace the interface movement. In addition, the introduction of the volume-of-fluid function mathematically formulates the surface tension force as a body force therefore the interfacial boundary condition becomes an additional force term in the momentum equations. The modified Navier-Stokes equations coupled with the volume-of-fluid function are then solved by an advanced finite difference scheme fully accounting for surface tension, wall adhesion, fluid momentum and viscous stresses. The location and slope of the fluid interface at the stop valve are not specified but are automatically evaluated as part of the solution process.

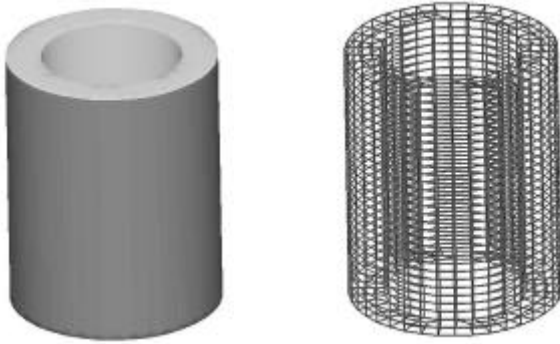


Figure 2. Geometry and mesh of the circular opening.

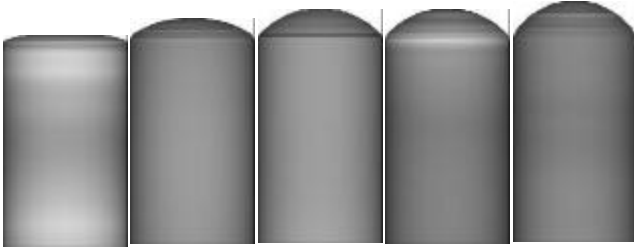


Figure 3: Transient simulations of meniscus growth. The radius of the pipe is 60 mm, surface tension 37 gm/s², applied pressure 863 Pa. From left to right the images are taken at 10 ms, 40 ms, 70 ms, 100 ms and 160 ms.

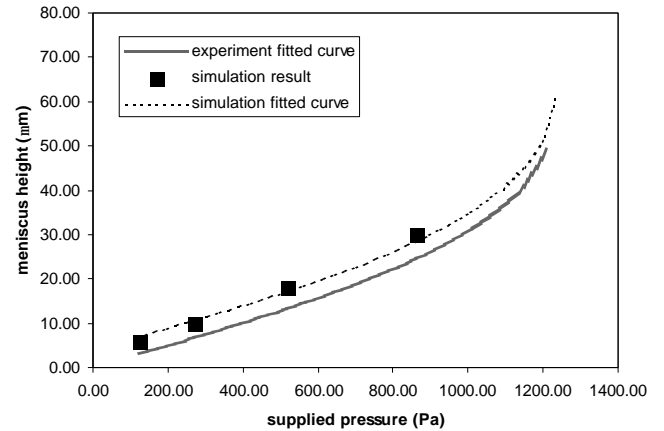


Figure 4: Meniscus height versus supplied pressure.

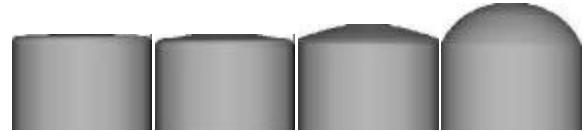


Figure 5: Meniscus shapes at steady state (simulation results). The supplied liquid pressures are 123 Pa, 271 Pa, 518 Pa and 863 Pa respectively from left to right.

WORKING RELATION OF FLUIDIC CAPACITANCE

As the meniscus area/volume enlarges with increasing driving pressure, the increase in interfacial surface energy appears as an equivalent capacitance in the fluidic circuit. Such capacitance-like behavior model can be extracted from detailed simulations, as shown in following example.

The opening of the channel is assumed circular and is pneumatically pressurized. Fig. 2 shows the geometry and mesh of the device in detailed simulation. A meniscus grows at the top of the opening. The height of the meniscus H represents the volumetric response of the meniscus to the driving pressure.

Fig. 3 shows a sequence of simulation results of meniscus growth in a transient process. When time equals to 160 μ s the pressure is uniform except for oscillations at the interface. At this point the steady state is considered achieved and the height of the meniscus is measured as the response of this fluidic capacitance.

The height of the meniscus is plotted against the applied pressure in Fig. 4, and compared against experimental measurements (Moroney et al 1998). The comparison between simulation and experiment is quite good, especially in the predicted trend. A possible source of the shift between the experiments and the simulations is the meniscus oscillation, which creates difficulties in measurement both in experiment and numerical simulations. In the numerical simulations the height of the meniscus is measured at its maximum – resulting in the shift higher than experiments. Based on analytical solution (equation 1) and simulation results, a fitted curve is given as

$$H = H_0 + \frac{2g_{la}}{P_m} \left(1 - \sqrt{1 - \left(\frac{DP}{4g_{la}} \right)^2} \right) \quad (3)$$

where the offset $H_0 = 4$ micron, representing the working relation of the fluidic capacitance (Fig. 4). The offset H_0 stands for the energy loss due to meniscus oscillation and viscous dissipation.

The interfacial contact at the rim of the opening modifies the shape of the meniscus therefore local curvature ϵ . Adjusting the geometry of the abrupt opening (illustrated in Fig. 6) may change the local contact at the rim and consequently the capacitance working relation (Man et al 1998). When the angle β increases, the “effective” contact angle decreases. The same volume of the meniscus effectively holds less surface energy. Therefore under the same supplied pressure, the meniscus height is expected to increase with β . Working relation of the capacitance accounting for β is plotted in Fig. 7. Analytical analysis of such type is fairly complex. Data points in Fig. 7 are obtained from simulations. Based on the simulation results, taking into account that the capillary barrier disappears when $\beta=90^\circ$, the fluidic capacitance model is further amended to

$$H = \left(H_0 + \frac{2g_{la}}{P_m} \left(1 - \sqrt{1 - \left(\frac{DP}{4g_{la}} \right)^2} \right) \right) / \cos b \quad (4)$$

accounting for the geometry of the capillary opening.

MAXIMUM CAPILLARY BARRIER

The maximum capillary barrier P_{cb} defines the breaking point of this micro-fluidic capacitance. When the supplied pressure exceeds P_{cb} , a fluid flow will be re-established, or, this fluidic capacitance will be “shorted”. This parameter is important to applications that require prevention of flooding in selected parts of a micro-fluidic system and sample injection at a specific time during reaction. It defines the working limitation of the gating operation.

An example highlighting the capillary barrier extraction is a capillary-driven valve pumped by centrifugal force. Centrifugal driven μ TAS devices have attracted noticeable attention recently and become one of the major themes in contemporary μ TAS research (van den Berg et al 2000). A typical device consists of several structures such as in Fig. 8 distributed

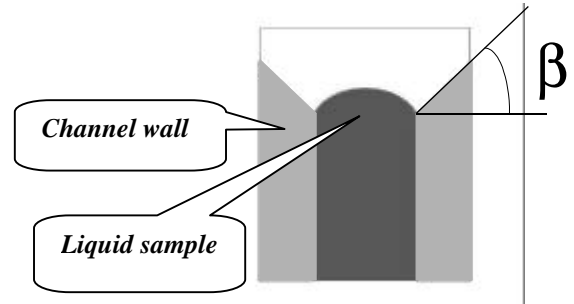


Figure 6: Sketch of the capillary opening.

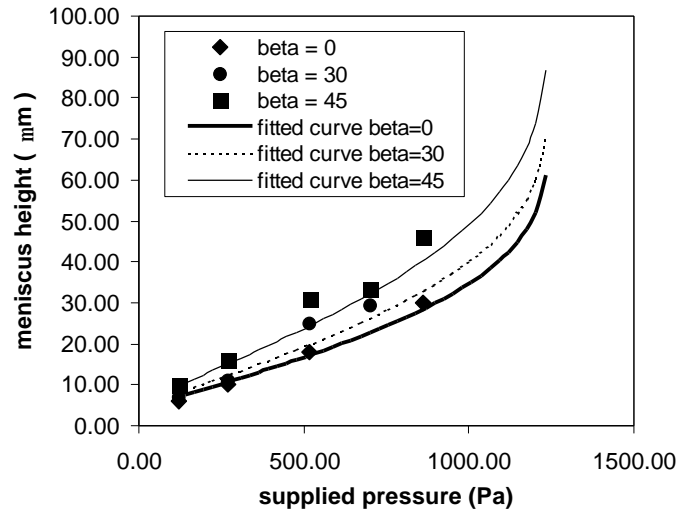


Figure 7: Capacitance model accounting for the variation of b (simulation results).

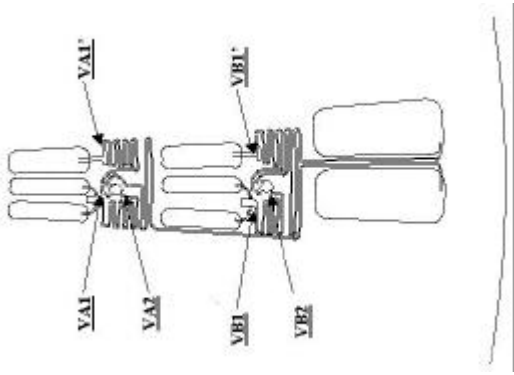


Figure 8: A slice of detailed micro-fluidic structure positioning on the rotating plate radically. Fluids flow and combine from the reservoirs at top in two stages, gated by the junctions marked with the "V"s. (courtesy Dr. Gregory J. Kellogg).

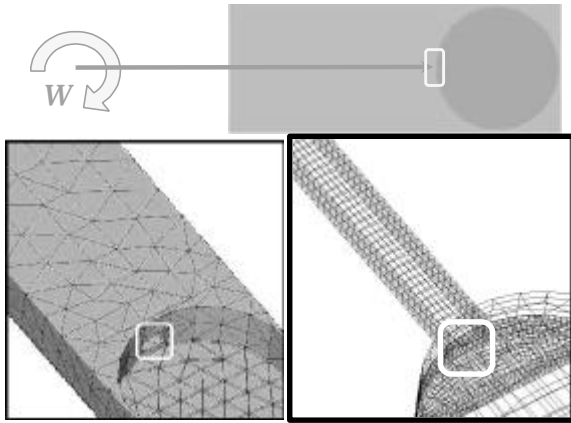


Figure 9: Capillary-driven valves in rotating disk devices. The carton at top illustrates the rotating mechanism. Lower two images show the meshes used in simulations. The left is of the solid device, the right is of the fluids.

radially on a rotating disk (Duffy et al 1999). The device is composed of fluid reservoirs, transport channels and reaction chambers. When the plate rotates, the centrifugal force builds up a pressure gradient inside the liquid with maximum liquid pressure at the meniscus, denoted by P_m in Fig. 1.

When the liquid momentum is considered negligible, the Navier-Stokes equations reduce to a balance between the centrifugal force and the pressure gradient. Therefore P_m can be expressed as $\rho\omega^2 r\Delta r$, where r is the average distance from the liquid element including both in the reservoir and in the connecting channel to the rotating center, Δr the radial length that the liquid sample occupies. When the rotating speed ω exceeds certain threshold value ω_{max} , the maximum pressure that the meniscus can sustain is reached. This pressure is the maximum capillary barrier, P_{cb} ,

$$P_{cb} = \rho\omega_{max}^2 r\Delta r. \quad (5)$$

Fig. 9 illustrates the computational model used in the simulation. The abrupt opening is highlighted. The duct has a rectangular cross-section in this case, which is more typical of microfabricated devices.

The transient meniscus formation process is shown in Fig. 10. The top row shows the meniscus shape at the opening. A slice plane is cut through the liquid body from the meniscus to the reservoir. The bottom row shows the pressure distribution at that slice plane. From left to right the time is 0.0, 1.62, 3.28 and 10.28. The time unit is given by surface tension and hydraulic diameter of the opening. The pressure distribution shows when time=10.28, a steady state is achieved.

To identify the maximum capillary bearing, the rotation speed is gradually increased until the liquid sample breaks the capillary barrier and floods into the reaction chamber, as shown in Fig. 11. A numerical probe is immersed into the liquid just below the meniscus and the radial velocity of the interface is recorded. If the centrifugal force is less than the capillary bearing, the liquid velocity gradually damps to zero as the meniscus oscillates and comes to rest. The meniscus profile and the meniscus velocity history recorded by the probe are used together to identify the maximum capillary barrier.

The maximum capillary barrier strongly depends on the dimension of the capillary opening, represented by D_H , the hydraulic diameter of the opening. The dependency of the yield maximum capillary barrier on D_H is shown in Fig. 12. The simulation results are plotted against experimental data (Duffy et al 1999). The experiments and simulations agree quite well as the figure shows.

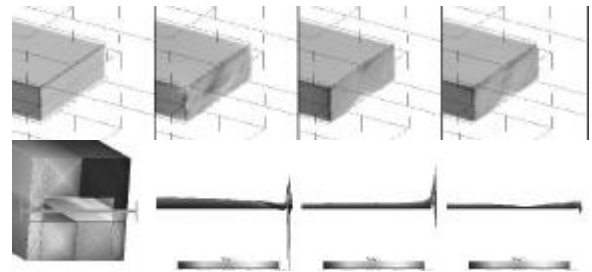


Figure 10: A typical transient process of meniscus formation (simulation results). Top row shows the shape of the meniscus, bottom row shows pressure distribution at a slide plane.

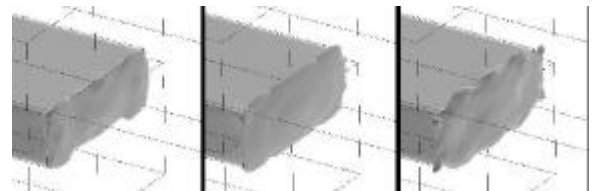


Figure 11: Breaking the capillary barrier. The driving pressure $\rho\omega^2 r\Delta r = 1719.12 \text{ Pa}$. From left to right the non-dimensional time is 1.17, 1.62 and 3.10.

$$P_{cb} = \frac{4g_{la} \sin q_c}{D_H} + g_{la} \sin q_c \left(\frac{1}{D_H} - \frac{1}{D_0} \right) \quad (7)$$

where $D_0=40\mu\text{m}$.

Additional cross-sections can be computed and correlation developed using a similar methodology.

CONCLUSIONS

In this article we present a micro-fluidic valve utilizing capillary effects and methodology to design and analysis of such type of micro-fluidic control mechanism. A multi-phase flow simulation technique is integrated into FlumeCAD to perform detailed simulations. Comparison with experiment is used to validate the numerical analysis and shows good agreement. Based on the simulations, a fluidic capacitance model is developed to characterize this gating mechanism. Micro-fluidic valves driven by liquid pressure and centrifugal force are analyzed as examples to show the method to extract the capacitance working relation and the ceiling condition. This fluidic capacitance model can be further incorporated into models for the devices that use these valves as a gating component. Similar procedures can be used to develop for other applications where capillary gating is a desirable effect.

ACKNOWLEDGMENTS

The authors wish to express their gratitude to Dr. Gregory J. Kellogg for useful discussion regarding to their experiments and the figure of their micro-fluidic centrifugal device (Fig. 8).

This study has been supported in part by Defense Advanced Research Projects Agency (DARPA) Composite CAD program under FlumeCAD (Grant no. F30602-98-2-0151) and NetFlow (Grant no. F30602-96-2-0306).

REFERENCES

- Bousse, L. , Minalla, A., Deshpande, M., Greiner, K. B. and Gilbert, J. R., 1999, "Optimization of Sample Injection Components in Electro-kinetic Micro-fluidic Systems", 12th IEEE International Conference on Micro Electro Mechanical Systems, Orlando, Florida, January 17-21 1999
- Duffy, D. C., et al, 1999, "Microfabricated Centrifugal Microfluidic Systems: Characterization and Multiple Enzymatic Assays", Analytical Chemistry 71, 20
- Ermakov, S. V., Jacobson, S., C. Ramsey, J., M., 1998, "Computer Simulations for Microchip Electrophoresis", μ TAS 1998 workshop, Banff, Canada, October 13-16 1998
- Harrison, D. J. and van den Berg, A., 1998, Eds. "Micro Total Analysis Systems '98", Kluwer Academic Publishers
- Hirt, C. W., and Nichols, B. D., 1981, "Volume of Fluid (VOF) Method for the Dynamics of Free Boundaries", Journal of Computational Physics, Vol. 39, pp. 201-225
- Hirt, C. W., 1999, "Direct Computation of Dynamic Contact Angles and Contact Lines", 3rd European Coating Symposium (ECS '99), Sept. 7-10, 1999
- Hsing, I.-M., Srinivasan, R., Harold, M. P., Jensen, K. F. and Schmidt, M. A., 2000, "Simulation of Micromachined Chemical Reactors for Heterogeneous Partial Oxidation Reactions", Chem. Eng. Sci., 55, 1

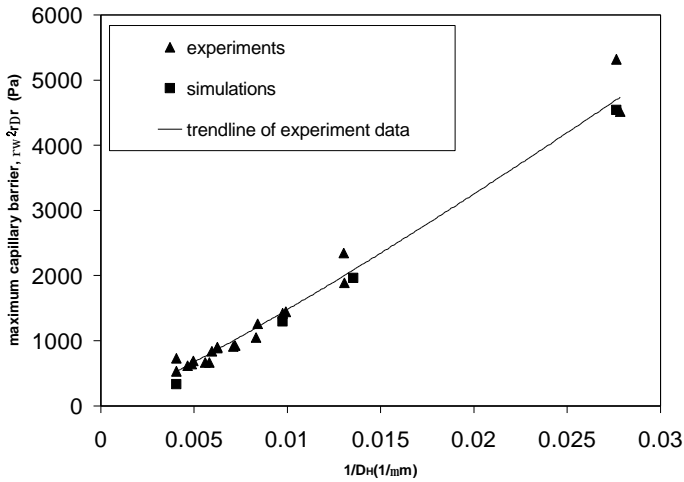


Figure 12: Maximum Capillary barrier versus different geometry of the opening (comparison between simulations and experiments).

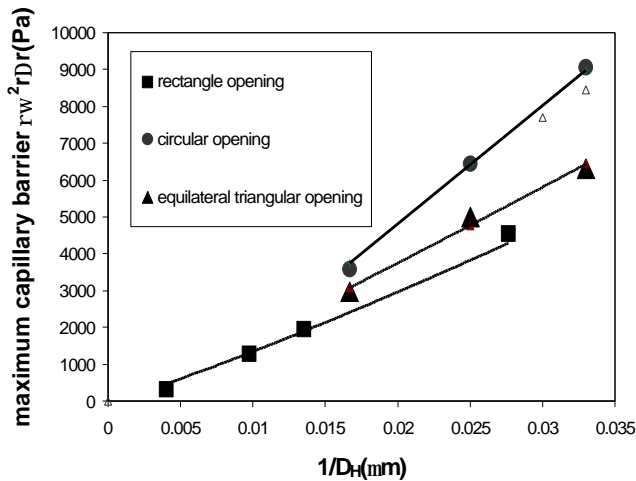


Figure 13: Maximum capillary barrier versus devices with capillary opening of different geometrical shape (simulation results).

Since the hydraulic diameter is chosen as the characteristic length, one would expect that the geometry of the opening would not have a significant effect on the capillary bearing pressure. Simulations were conducted to verify this dependence. The results indicate that the geometrical effect of the opening is not negligible and the analytical prediction of maximum capillary barrier (equation 2) is not adequate to represent this effect. To account for this variation, the model representing the capillary behaviour is modified as

$$P_{cb} = 4g_{la} \sin q_c (D_H)^n \quad (6)$$

where $n=-1.08$ for duct with equilateral triangular cross-section, $n=-1.14$ for duct with rectangular cross-section. An additional term is present in the reduced-order model for pipe flow,

Jensen, K. F., 2000, "The Impact of MEMS on the Chemical and Pharmaceutical Industries", Solid-State Sensor and Actuator Workshop, Hilton Head Island, South Carolina, June 4-8, 2000

Kim, E., and Whitesides, G. M., 1997, "Imbibition and Flow of Wetting Liquids in Noncircular Capillaries", *The Journal of Physical Chemistry B*, Vol. 101, No. 6, pp.855-863

Man, P. F., Mastrangelo, C. H., Burns, M. A., and Burke, D. T., 1998, "Microfabricated Capillary-Driven Stop Valve and Sample Injector", 11th Annual International Workshop on Micro Electro Mechanical Systems, Heidelberg, Germany, January 25-29, 1998

Moroney, R., M., Amantea, R., and McBride, S., E., 1999, "A Passive Fluid Valve Element for a High-Density Chemical Synthesis Machine", 2nd International Conference on Modeling and Simulation of Microsystems, San Juan, Puerto Rico, April 19-21, 1999

Olsson, A., Stemme, G., and Stemme, E., 1999, "Numerical Simulations of Flat-walled Diffuser Elements for Valve-less Micropumps", 2nd International Conference on Modeling and Simulation of Microsystems, San Juan, Puerto Rico, April 19-21, 1999

Oron, A., Davis, S. H. and Bankoff, S. G., 1997, "Long-Scale Evolution of Thin Liquid Films", *Reviews of Modern Physics*, Vol. 69, No. 3, pp.931-980

Patankar, N., A., and Hu, H., H., 1998, "Numerical Simulation of Electro-osmotic Flow", *Analytical Chemistry* 70(9), pp. 1870-1881

Shikhmurzaev, Y. D., 1996, "Dynamic Contact Angles and Flow in Vicinity of Moving Contact Line", *AIChE Journal*, Vol. 42, No. 3, pp.601-612

Van den Berg, A., Olthuis, W. and Bergveld, P., 2000, Eds. "Micro Total Analysis Systems 2000", Kluwer Academic Publishers

Zeng, J., Banerjee, D., Deshpande, M., Gilbert, J., Duffy, D. and Kellogg, G., 2000, "Design Analyses of Capillary Burst Valves in Centrifugal Micro-fluidics", μ TAS 2000 symposium, Enschede, The Netherlands, May 14-18 2000